Application of Serial Sectioning FIB/SEM Nano-Tomography in the Comprehensive Analysis of Arrays of Metal Nanotubes

Richard Phelan, Nikolay Petkov, Justin D. Holmes

Abstract

The ever increasing interest in nanostructured materials and shrinking dimensions of state-of-the-art devices pose new challenges both in synthesis and metrology. Although an extensive range of nanotubular materials of different compositions and for various applications are reported in the literature, often detailed structural characterisation of these materials is limited. This is due to the fact that techniques and characterisation protocols for structural analysis of "buried" nano-scale features, defects or inhomogenities that are difficult to obtain by conventional imaging methods, are still not fully developed. In the case of 1D nanoporous structures, the continuity of the nano-tubular channels, their uniformity and orientation is of particular interest. Herein, we employ a serial sectioning technique on a dual beam FIB followed by 3D volume reconstruction for comprehensive analysis of tubular metal nanostructures encapsulated within porous anodic alumina. Using this technique we demonstrate a nano-tomography characterisation protocol that can be used for analysis of nanoporous structures with emphasis on their channel uniformity and orientation. We specifically chose to examine Cu-nanotubes, deposited electrochemically within anodic alumina template, because there is great deal of debate regarding the deposition process. Hence the comprehensive analysis of the obtained structures will not only showcase the applicability of the developed characterisation methodology but will also, in conjunction with other advanced electron microscopy methods such as elemental nano-mapping on a scanning transmission electron microscope (STEM), provide conclusive evidence of the key factors at play during the deposition process.

Introduction

Ever since Martin *et al*. first reported the membrane templated synthesis of gold nanotubes,[1] the generation of nanotubes composed of a variety of materials has become a rapidly advancing field of study. One of the primary reasons for this advance is the potential ability to develop devices

with wide ranging applications, from nanoelectronics[2] through to biosensing.[3] Many routes for fabricating tubular structures within the templating matrices have been explored, including; electrochemical deposition (ECD),[1,4-6] electroless deposition (ED),[7,8] atomic layer deposition (ALD),[9-11] molecular beam epitaxy (MBE),[12] and sol-gel chemistries.[13-15] Specifically, these types of synthesis methods result in embedded morphologies with critical dimensions, orientations and complexity buried within the templating matrix. Consequently, there is a clear need to develop tools and techniques to explore the complexity, both structural and compositional, of such nanostructures within the template.

A standard imaging protocol when analysing structures embedded within aforementioned templates is based on acquiring secondary electrons using SEM with the electron beam perpendicular to the template surface or at some oblique tilt angles. In this case the information regarding the nanotube morphology is gathered from only several tens of nanometers depending on the acceleration voltage used and the tilt angles. This information is only representative for the nanotube start (or end points) but not for the full length of the nanotube which may exceed several micrometers. Another imaging protocol uses cross-sectional analysis where the template (membrane) is cut in two and the structures are imaged along their long axis within the template. This technique suffers from the inability to obtain a precise cross-section of the nanotubes themselves thus hindering the analysis of their interior. Moreover, it is often seen that nanotubes or nanowires tend to delaminate from the templating matrix in an incontrollable fashion.

Alternatively, the nanotube morphology can be visualised by using TEM after dispersing the nanotubes on a TEM grid. This is of course only possible after removing the templating matrix in a suitable solvent and forming a stable suspension. Depending on the type of the nanotubes synthesised and template used this process can be quite laborious and prone to artefacts. Furthermore, metal nanotubes with large (more than 100 nm) external diameters would be very difficult to analyse due the limited electron transparency. Hence, the interface surface between the nanotubes and the templating matrix, or any other buried nano-sized inhomogeneties are not accessible for analysis. A more elegant method for analysis is to obtain thin foils perpendicular to the long axis of the embedded structures by ion-milling and examine them by TEM. However in this case the sampling length is only several tens of nanometers limited by the necessity to obtain electron transparent foils.

It has been demonstrated that serial sectioning on a FIB/SEM (Dual Beam or Cross Beam) instrument, and can be used to determine the orientation and buried structural inhomogenities along the direction of 1D nanoporous materials (ref). Because of the added directionality in the analysis (milling direction is at a set angle towards the plane of the SEM image) 3D information can be obtained rendering this technique as tomography. With the ever increasing imaging and milling resolution of both the electron and the Ga-ion columns respectively, the technique can truly be named as nano-tomography.

Briefly, in the FIB/SEM nano-tomography methodology, a clean surface is milled away and imaged by the SEM in a sequential fashion thus creating a stack of images (Figure 1). The plane of the SEM image defines the *x*- and *y*-directions of the image stack while the milling direction defines the depth (*z*-direction) of the stack. For high resolution FIB-tomography the thickness of the removed material in *z*-direction should be of similar magnitude to the pixel resolution in the *x*-*y*-imaging plane, i.e. the higher the imaging resolution in *x*-*y* plane, the more precise the milling process should be with thicknesses of the slices reaching sub-10 nm. Hence this makes the technique very time consuming and difficult to execute when large (several tens of micrometers) volumes are analysed. Another limitation to the process is imposed by the drift that is either caused by mechanical or electromagnetic instabilities of the system. Thus precise control over the Ga-ion milling process and the drift during the serial sectioning should be attained. This is now possible with the new generation of high stability / high flux Ga-ion columns and high stability FIB stages. The final phase of the FIB nano-tomography is to use the obtained stack of SEM images to reconstruct a 3D volume. This is done by applying different algorithms for image alignment, image rendering and segmentation, contrast enhancement or noise suppression. Further details on this process can be found elsewhere (ref). Most importantly the 3D image reconstruction has to be performed with caution so that various possible artefacts are avoided and that the obtained 3D map reflects accurately the 3D structure of the examined material.

In this report we show that serial sectioning FIB/SEM nano-tomography can be applied for revealing the “true” structure of Cu nanotube structures embedded as arrays within anodic alumina oxide (AAO) template. Two distinct types of specimens were analyzed having complex nanotube structures and it is demonstrated that false misinterpretation of the nanotube morphologies can be avoided by using this technique. Detailed description of a nano-

tomography protocol for analysis of 1D nanoporous materials, their orientation, continuinity and dimensional analysis is presented. Elemental nano-mapping on a STEM-EDX system and HAADF imaging supplied further insight into the morphology and composition of the embedded structures that helped in determining the key factors at play that need to be considered during the depositions.

Experimental

Electrochemical depositions

Anodic alumina membranes of nominal pore size 200nm (Whatman, working area of 1cm, pore diameter of about 200 nm, thickness 50-70 μm) were placed into a 100 ml round bottomed flask for silylation. Two silylation agents were used, namely 1ml of either Trimethoxysilylpropyl-diethylenetriamine (Fluorochem) (Sample A) or N-(trimethoxysilyproply) ethylenediamine triacetic acid tri-sodium salt, 45% in water (ABCR) (Sample B) In the latest case, the pH of the aqueous solution was adjusted to 2 with 37% HCL. The membranes were refluxed at 100°C for several hours and then washed with distilled water or toluene, respectively. A thick (> 300 nm) gold layer was sputtered onto one side of the membrane to serve as a working electrode. Ammonia-citrate, copper electrolyte was employed for the deposition, containing; 0.1 M $CuSO_4$, and 0.12 M $Na_3C_6H_5O_7$ at pH 7 adjusted with ammonium hydroxide.[23] Electrodeposition was carried out galvanostatically using a two electrode electrochemical cell operated at 0.3 mA cm^{-2} for 24 hrs at room temperature. We specifically chose to examine Cu nanotubes formation, assisted by silane agents and deposited electrochemically within anodic alumina template, because there is great deal of debate regarding the key factors in the deposition process.

Conventional Imaging

Samples for plan-view SEM imaging were first prepared by using precision Ar-ion polishing performed at grazing angles of 5 degrees at 5 kV using a Gatan, precision ion polishing system (PIPS), model 691. The surface morphology of the composite anodic alumina/Cu nanotube samples was imaged by a JEOL, JSM 65007 SEM or an FEI Nova NanoSEM. Samples for STEM imaging were prepared Dual Beam FIB *in-situ* lift-out. HAADF STEM imaging and EDX analysis was obtained using a JEOL 2100 STEM equipped with an Oxford instruments, INCA 250, EDX detector and a dedicated drift correction system.

FIB/SEM nano-tomography

FIB serial sectioning and SEM imaging was performed on a FEI Helios, NanoLab Dual Beam system equipped with Tomahawk ™ Ga-ion column and piezo-driven high stability stage. Samples for serial sectioning FIB nano-tomography were prepared by depositing Pt protection layer by electron beam induced deposition, followed by ion-beam induced deposition of 2 µm thick protective Pt layer close to the side where the Au electrode was deposited (see Figure 1 b). After choosing markers that were used for *x*-, *y*-, and *z*-drift corrections, the serial sectioning was accomplished using a Ga-ion beam current of 11 pA at 30 kV. A series of secondary electron SEM images were acquired at 5 kV using an electron beam current of 43 pA, with calibrated maximum resolving power of 1.1 nm using in-lens secondary electron detection and Constant Power™ design of electromagnetic lenses. Each cycle of manual drift correction/sectioning/imaging took around 30 s. Normally 50 – 60 cycles were performed with an average thickness of 6 - 7 nm for each milled section. Thus, the smallest structural element of interest that can be visualised by using 3D reconstruction would have critical dimensions of about 60 – 70 nm in the *z*-direction (ref). Major precautions were taken to minimize ion-beam drift (drift in *z/x* plane) which results in varying thickness of the milled slices. Such problems would result in image stacks varying thicknesses of the slices and would create difficulty in defining the voxel size in the *z*-direction. Automated drift correction involves acquisition of reference images with the FIB. These are acquired at higher beam current than that used for serial sectioning, and as such requires switching between apertures. It was found that such a procedure causes more system instability and hence the introduction of artefacts during serial section, than if manual drift correction is performed with the same ion-beam current over shorter image acquisition times (50 ms). Additionally, abrupt brightness and contrast variations from image to image in the stack due to sample charging were minimised by working at lower electron beam currents. It should be mentioned that ion-beam and stage stability of the Helios NanoLab system is far superior to older versions of the FEI family of Dual Beam systems and as such allows for reduced drift and beam discharge during sequential milling and imaging. We note that due to the Constant Power™ design of electromagnetic lenses, high controllability and reproducibility of the electron beam, stacks of high resolution SEM images with minimized drift and brightness/contrast changes were obtained.

3D image reconstruction

Image processing and 3D reconstruction includes the following steps: (a) correction of voxel dimensions for oblique-angle imaging (52 degrees), (b) digital image alignment to compensate for *x–y* drift (image registration); (c) crop-out of a suitable sub-volume; (d) image segmentation/binarization; and (e) 3D visualization and representation. Here, all the steps of the data processing were performed using the Amira 3.1 software package. Image registration and segmentation are amongst the most important stages in such a procedure. Namely, an iterative approach is applied starting with manual alignment of the image stack and finishing with least square alignment method until optimal quality factor is obtained. This was followed by cropping-out a region and further image alignment in order to obtain *x-y* image alignment with sub-10 nm resolution and quality function close to 100 %. Different image segmentation procedures were examined including threshold segmentation and interactive manual segmentation; the second one although much more time consuming showed better results.

Results and Discussion

Conventional SEM imaging

To date several groups have reported various means of generating arrays of Cu nanotubes within anodic alumina templates, highlighting the importance of having a perforated back electrode (a conductive coating forming only around the mouth of the AAO pores, without sealing them) together with modification of the anodic alumina walls in order to obtain successful synthesis (ref). In order to comprehensively investigate such structures we have electrodeposited Cu within AAO after sylilation of the template surface with chelating agents and followed by Au metal sputtering to form continuous back electrode layer. After the synthesis we performed standard SEM imaging of the nanotube start points (after Ar-polishing of the back electrode). Figure 2 shows representative examples of such areas together with the cross-sectional images obtained after cutting the membranes in two. These fast and inexpensive sample preparation methods gave us the opportunity to investigate large sample regions across the membrane surface and to obtain an overall understanding of the deposition process, as well as to compare our results to the other published synthetic methods. Based on this type of analysis it can be concluded that in sample A (Figure 2 a and b), Cu-nanotubes were successfully generated and that these displayed a uniform, tubular morphology with loading factors reaching 100%. The dimensions and shape of tube openings are varying with the shape of the confining AAO pores,

but the overall thickness of the tube walls is almost constant. Sample B (Figure 2 b) showed that about 50 – 80 % of the nanostructures generated displayed a tubular morphology with structures appearing less uniform with smaller inner diameters and larger walls. The presence of more than one opening per tube was also observed, with some pores as small as 20 nm. The SEM cross-sectional analysis (Figures 2 c and d) showed the total length of the Cu structures (5 and 2 μm, correspondingly) and that all of them are deposited to almost the same length within the AAO pores. It is important to stress that other reports based on similar types of images, confidently concluded successful deposition of nanotubular morphologies within AAO templates.

Serial Sectioning FIB/SEM nano-tomography

In order to conclusively establish whether or not the tubular morphology of the embedded Cu nanostructures is continuous along their entire length, 3D structural analysis by means of serial sectioning using Dual Beam FIB/SEM was undertaken. The analysis was performed as explained in the Experimental Section and schematically illustrated on Figure 1. Figure 3 shows a sequence of images extracted from the full stack of 3D data set after image cropping, alignment and registration for the two specimens under analysis. Full data sets can be visualised by uploading the whole series of images stacked into movie format (see Supplementary information). It is seen that for sample A, there is a remarkable change in the type of the embedded morphologies, beginning with well shaped tubular structures at the start points to structures with completely closed pore openings at their ends. Similarly a volume of interest from sample B was examined. In this case, the overall morphology of the embedded Cu structures e.g. nanotubes with smaller and less uniform openings (in some cases several openings within one tube) is preserved throughout the whole examined length (1200 nm). This unexpected difference clearly demonstrates that the additional structural information, along the "buried" longitudinal direction of the tubes, is indeed very important.

After image acquisition and post-acquisition processing (alignment, image translation and contrast/brightness adjustment as explained in the Experimental Section), 3D volume reconstruction was undertaken. The reconstructions viewed in two different directions for the Cu nanostrcutures corresponding to sample A, are shown in Figure 4. The reconstructions are obtained on 300x300x1000 nm physical volumes. The surrounding AAO matrix has been omitted during the 3D visualisation for clarity, thus living only the Cu structures with their

internal porosity. The 3D visualisation is presented by solid color for the images in (a) and (c) where the Cu is in cyan, and by transparent mask for images (b) and (d) where outlines of the pores within the Cu structures are easier to see. Hence, the reconstructions in a and c focus on the overall morphology, shape and pore openings of the Cu nanostructures, where as the reconstructions in b and d pinpoint the internal pore shape, uniformity and continuity. There are several distinct features that are immediately distinguishable in the 3D reconstructions shown in Figure 4: (i) there are Cu structures that are formed from several branches whereas each branch is a nanotube at its start (Figure 4 a), (ii) nanotubular morphologies are only seen at the pore mouths with the shape of the openings following the overall shape of the nanostructures (Figure 4 c), (iii) the pores are terminating at about 300 nm from the start point and are conical in shape (Figure 4 b and d),. Similarly 3D reconstructions were performed on 300x300x800nm physical volumes for two separate Cu nanostructures that belong to sample B (Figure 5). The reconstructions pinpoint the fact that pore openings with much smaller diameters are formed and that several pores are seen within the same Cu nanostructure (Figure 5 c). More importantly it is seen the expected tubular morphologies are not continuous; on the contrary, globular pores with varying dimensions and centred along the long axis of the Cu nanostructures are formed (Figure 5 b and d). Detailed qualitative analysis of the pore size distribution, pore volumes and surface areas of nanopores with radii higher than 50 nm can be determined by such reconstruction as shown by Holzer *et al (ref)*. Here we demonstrate that high resolution nano-tomography can be performed to visualise pores as small as 30 - 40 nm, with conical or globular shapes, and to quantitatively estimate their localisation and distribution along one-dimensional structures. This is made possible by considering the following limitations of the FIB/SEM nano-tomography performed on Helios, NanoLab instrument.

The primary limitation to consider is regarding the accuracy in determining the shape and dimensions of sub-50 nm pores. There are two major sources of error that need to be considered: (i) accuracy of determining the dimensions in the *x-y* planes that is directly related to the calibration of the electron-beam column, and (ii) accuracy in determining the dimensions of the *z*-direction that is related to the drift in the *z*-direction, and to the roughness of the polished thin slice by FIB milling. In our laboratory we use high resolution calibration standards for calibrating the magnification scale on our electron microscopy equipment which guaranties error on the magnification scale of less than 3%. The SEM images for high resolution 3D

reconstruction were acquired at 3.6 nm per pixel. Thus for images with such resolution the systematic error in determining dimensions of features in *x*-*y* planes is about 0.11 nm. The thickness of the slices polished away at the ion-beam current used (11 pA) is determined by calibrating the thickness against ten consecutive slices that are milled away in Cu and it is on the order of 6-7 nm. The roughness of such slices is dependent on the milling conditions used and the ion-beam settings (including astigmatism and focusing) but more importantly it depends largely on the resistance of the materials against milling. In our case the sample is heterogeneous composed of nano-scale alumina and copper components, and has internal nano-porosity. Thus the roughness of each slice is very difficult to estimate. Nevertheless, based on the STEM images of thin electron transparent foils (see Figure 6 and Supporting Information) no obvious variation in the thickness can be seen that might be attributed to large (more than 10 nm) variation in the roughness of the slices. Thus we estimate that the pixel size in z-direction is about 6 - 7 nm with possible systematic error that can be as high as 50%.

The other parameter that has large influence on the accuracy in determining the size and shape of the features during FIB/SEM nano-tomography is drift in the system. Although drift in the *x*- and *y*- directions is not a major concern as it can be corrected by digital alignment of the image stack using markers, the drift in the *z*-direction can have large influences on the variation in the thickness of polished away slices. Here we perform manual drift correction using digital markers for both electron (*x*-*y* plane) and ion-column (*z*- direction). It should be mentioned that measured drift rate in *z*-direction at the milling conditions used is about 2-3 nm/min, and it has been corrected at every third consecutive slice. Finally, the errors associated with the post-acquisition image processing and 3D image reconstruction (filtering, segmentation and registering) can be described roughly by the rule of thumb that a successful reconstruction is possible if the size of the reconstructed feature in 3D is a minimum of 8-10 times the size of the voxel in *z*-direction (ref). In our measurements the voxel size in *x* and *y* is 3.6 nm which restricts the smallest feature size that can be reliably reconstructed in 3D to 30 - 40 nm. The size of the z direction of the voxel is higher (6 - 7 nm) and suggests that features with dimensions below 60 nm will be reconstructed with high errors. For example, this will be important to consider in the case of sample B were pores with globular morphologies were observed. In this case only pores with critical dimensions in the *z*-direction (see Figure 6) showed that pores with dimensions of about 20 - 30 nm exist in those Cu nanostructures; hence the 3D reconstruction of those features

should be with highly erroneous On the other hand, the tomography methodology developed in this study was successful in analysing the 3D shape, dimensions, localisation and continuity of pores that have larger (more than 60 nm) critical dimensions in the *z*-direction such as the conical pores in sample A or the larger globular pores in sample B. It is believed that simlar 3D analysis can be successfully extended to one-dimensional porous systems ("truly" channelled systems such as mesoporous silica films, parallel anodic alumina films or block co-polymer films, ref) with pore diameters below 20 nm, and critical dimensions in the *z*-direction (along the long axis of the channels) higher than the limitations described disrobed herein. This will supply important information on the continuity, pore direction and correlation lengths of such systems that are essential for their implementation as functional units in designing novel devices for nano-fluidics, templates for interconnects or lithography masks (ref).

In order to verify the elemental composition and to give further insight into the formation process of the Cu nanostructures HAADF imaging followed by EDX mapping was employed. After obtaining a thin foil, analysis was performed with the electron beam parallel to the long axis of the Cu nanostructures. The sections were extracted from two different locations along the templating matrix e.g. (i) at a distance of about 150-200 nm from the back electrode and (ii) at a distance of about 600-650 nm from the back electrode. HAADF images together with the corresponding EDX maps for the first case are shown in the Figure 6 for samples A and B. For sample A, the HAADF imaging revealed structures of a tubular morphology (Figure 6 a) in correspondence of the SEM imaging, and no additional porosity within the Cu nanstructures. Due to the enhanced Z-contrast in the HAADF images the appearance of brighter rim on the outer surface of the Cu nanostructures was detected that can be attributed to high atomic number metal. The STEM–EDX mapping identified this as Au inner coating of the AAO template (Figures 6 b - d). The thickness of the Au rim determined from the elemental maps is estimated to be around 10 - 15 nm. When sections were extracted from areas at larger distance from the back electrode the structures showed no porosity (see Supplementary information) and no Au rim. This suggests that in the case of sample A the tubular nature of the Cu structures (seen only in the near vicinity to the electrode) can be associated with the formation of a thin coating of Au within the interior of the templating channels. The depth of such a coating within the AAO channels is difficult to be accurately estimated by serial sectioning FIB/SEM because of the small thickness of the Au rim and the fact that contrast variations in SEM are not directly related

to chemical composition, on the contrary, they can be a result of edge effects or other beam/sample interactions. Similar analysis was performed for sample B where the appearance of the Au coating within the AAO interior in areas close to the electrode is less pronounced or fully beyond the limit of detection both in the HAADF image and in the EDX maps (Figure e – h)). Consequently the occurrence of the seen morphologies can be attributed to the use of silane B, which acts to chelate Cu^{2+} ions thereby affecting the pre-concentration of metal ions at the pore walls and hence structures with globular pores all along the 1D Cu nanostructures.

Conclusions

A detailed description of a nano-tomography protocol, by the means of FIB/SEM serial sectional technique for analysis of nanoporous materials, their orientation, continuity and dimensional analysis is presented. The results show that the morphologies of structures deposited within AAO must be analysed with caution and when possible using advanced electron microscopy protocols such as electron tomography in order to obtain a comprehensive picture of the entire 3D structure. This is of particular concern when analysing structures that are deposited by techniques which may lead to unexpected morphologies and inhomogenities, or that are a result of deposition routes that are still under dispute. Most importantly, we have demonstrate that the cross-correlation of the results obtained by FIB/SEM serial sectioning and nano-scale (S)TEM EDX elemental mapping of selected foils can be used to give further insight into the deposition process of nanotubular morphologies within the AAO templates.

References: still to complete…

Figures

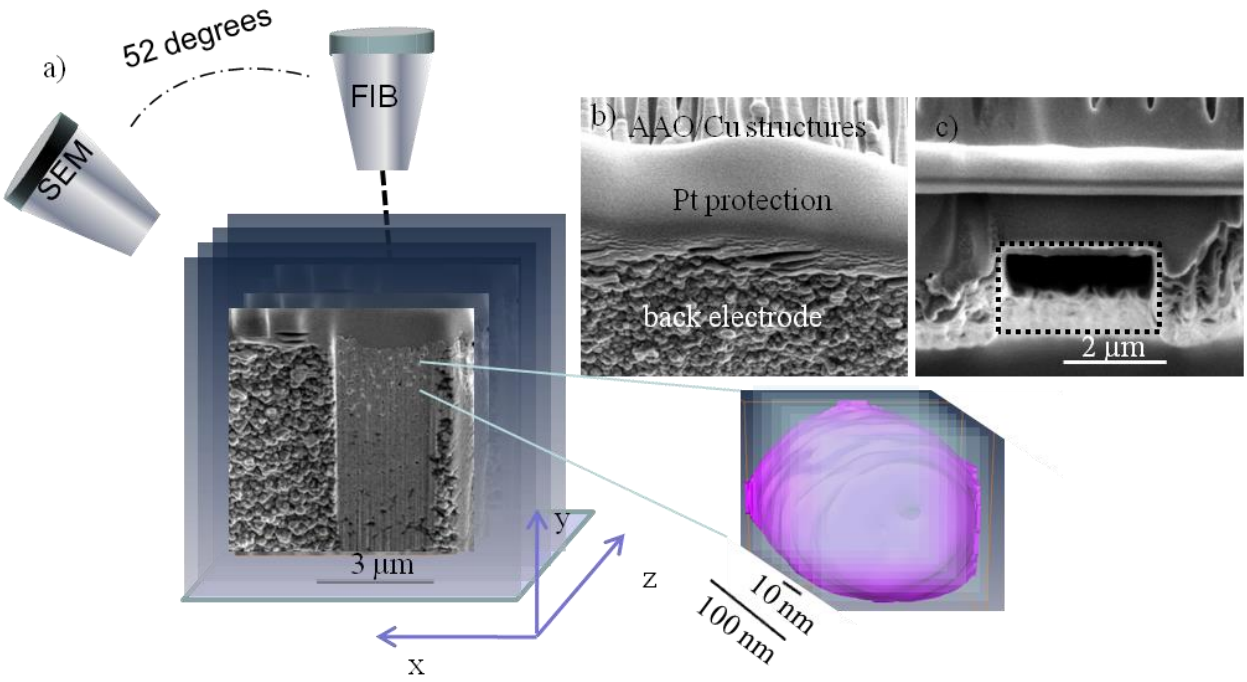

Figure 1. a) Schematics of the serial sectioning FIB/SEM nano-tomography method, b) tilt view SEM image of the AAO/Cu nanostructures before commencing serial sectioning featuring continuous Au back electrode and Pt protection, c) Ga-ion beam image of the same area after serial sectioning showing milled away volume of material starting from the back electrode with the corresponding markers for correction of the drift on the ion-beam column.

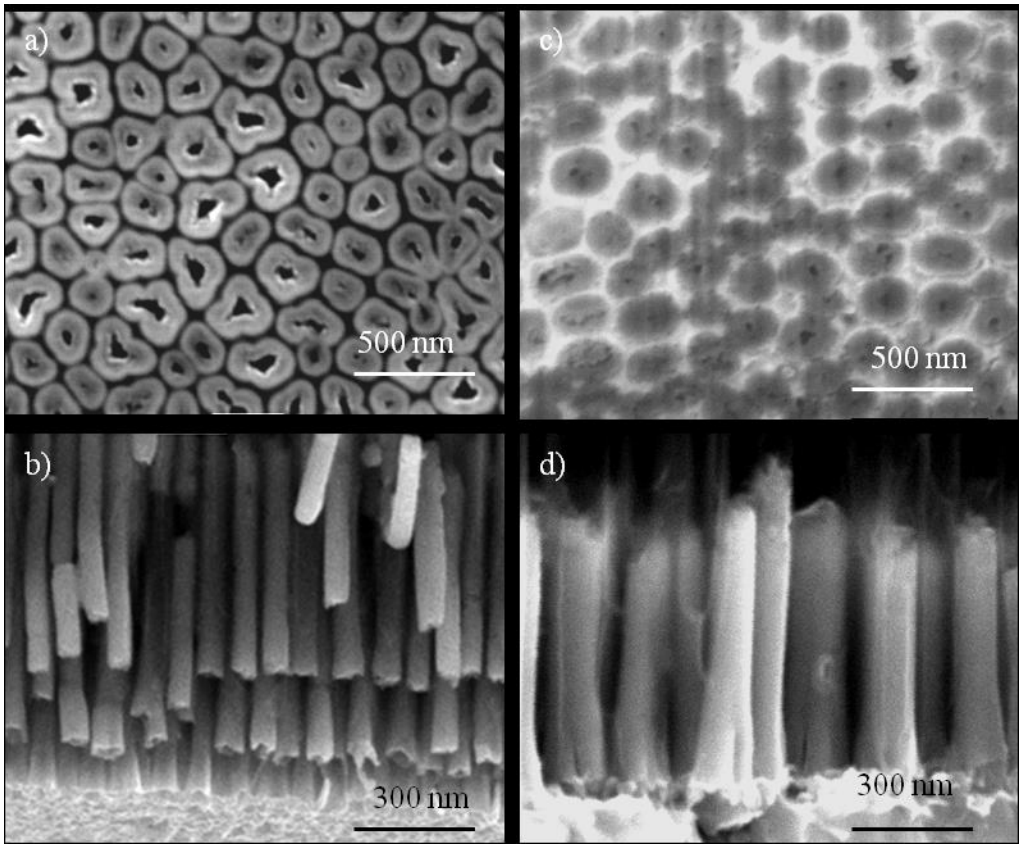

Figure 2. Plan view SEM images of Cu nanostructures embedded within AAO for a) sample A and c) sample B, and cross-sectional views obtain after cutting the samples in two for b) sample A and d) sample B.

Figure 3.

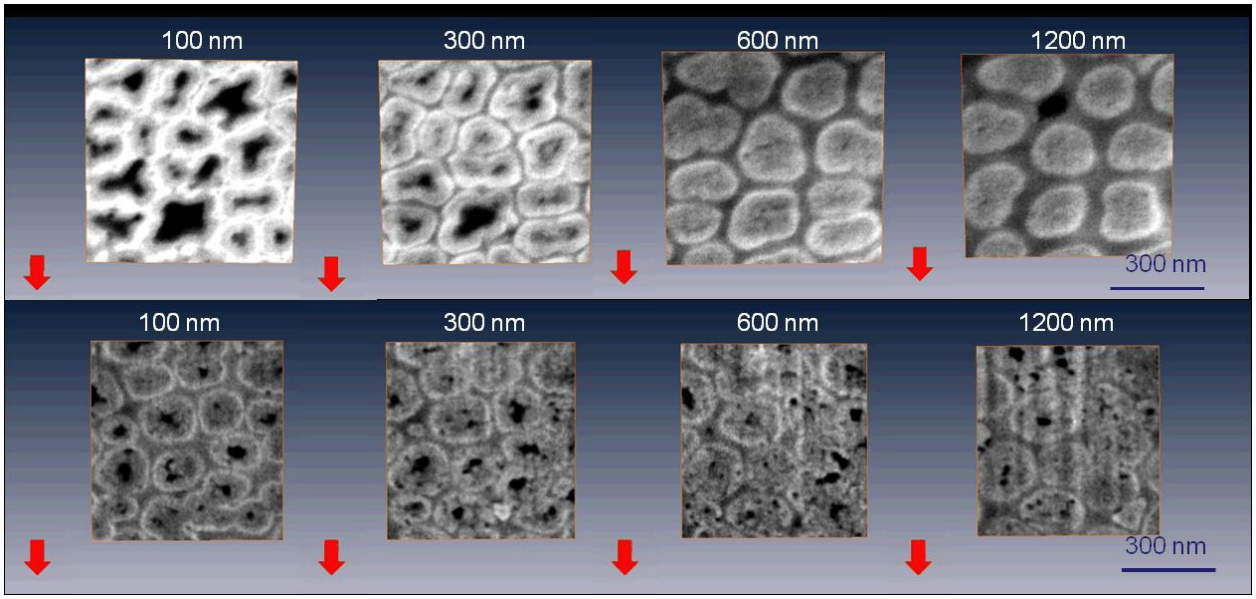

Figure 3 Series of plan view SEM images taken at four different lengths from the back electrode obtain after sequential FIB milling. The upper and bottom rows correspond to sample A and B.

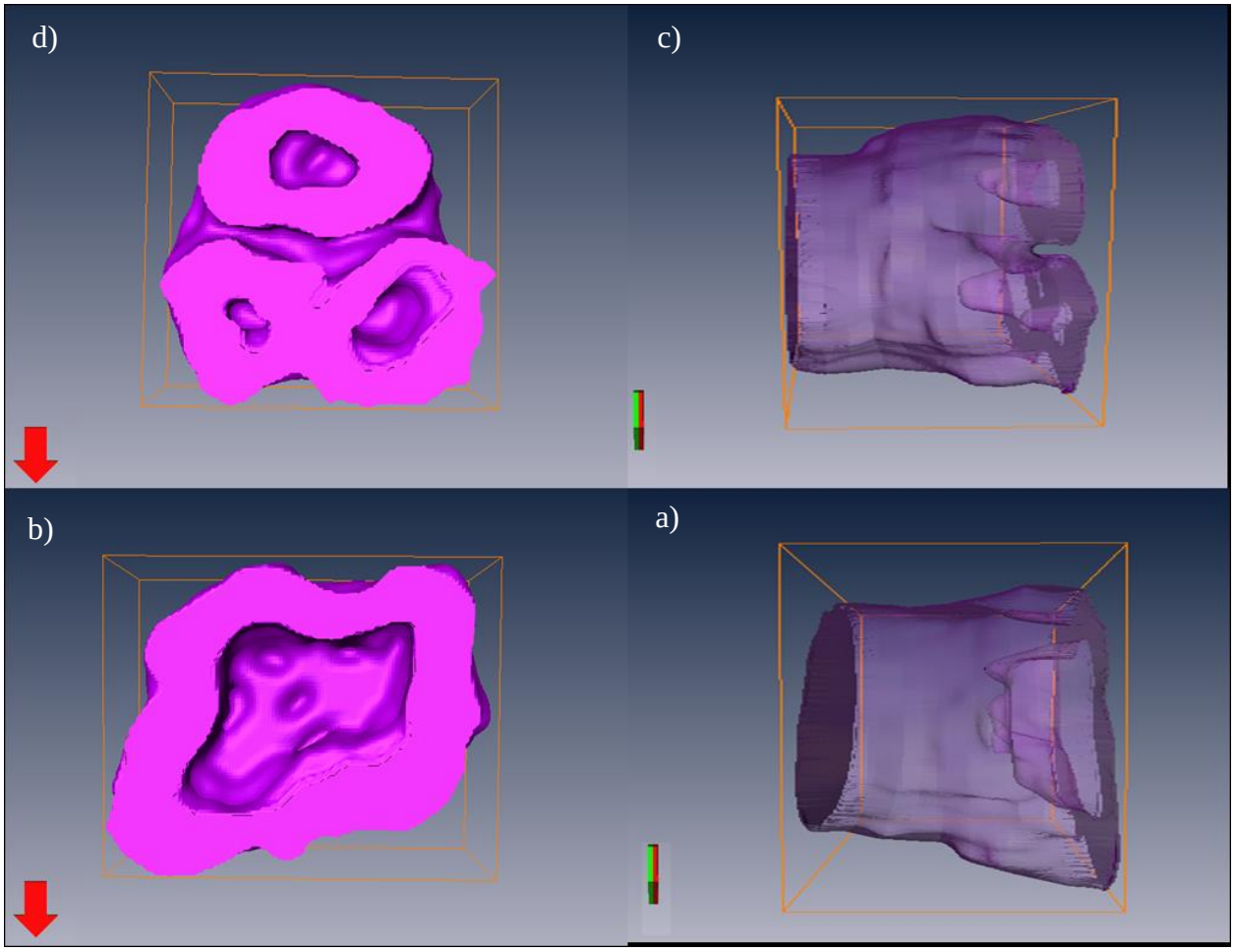

Figure 4. 3D reconstructions for two different Cu nanostructures (upper and bottom rows) corresponding to sample A. Two visual representations of one and the same nanostructure are shown a) and c) in solid color, and b) and c) transparent and rotated by 90 degrees. The surrounding AAO matrix is omitted for clarity.

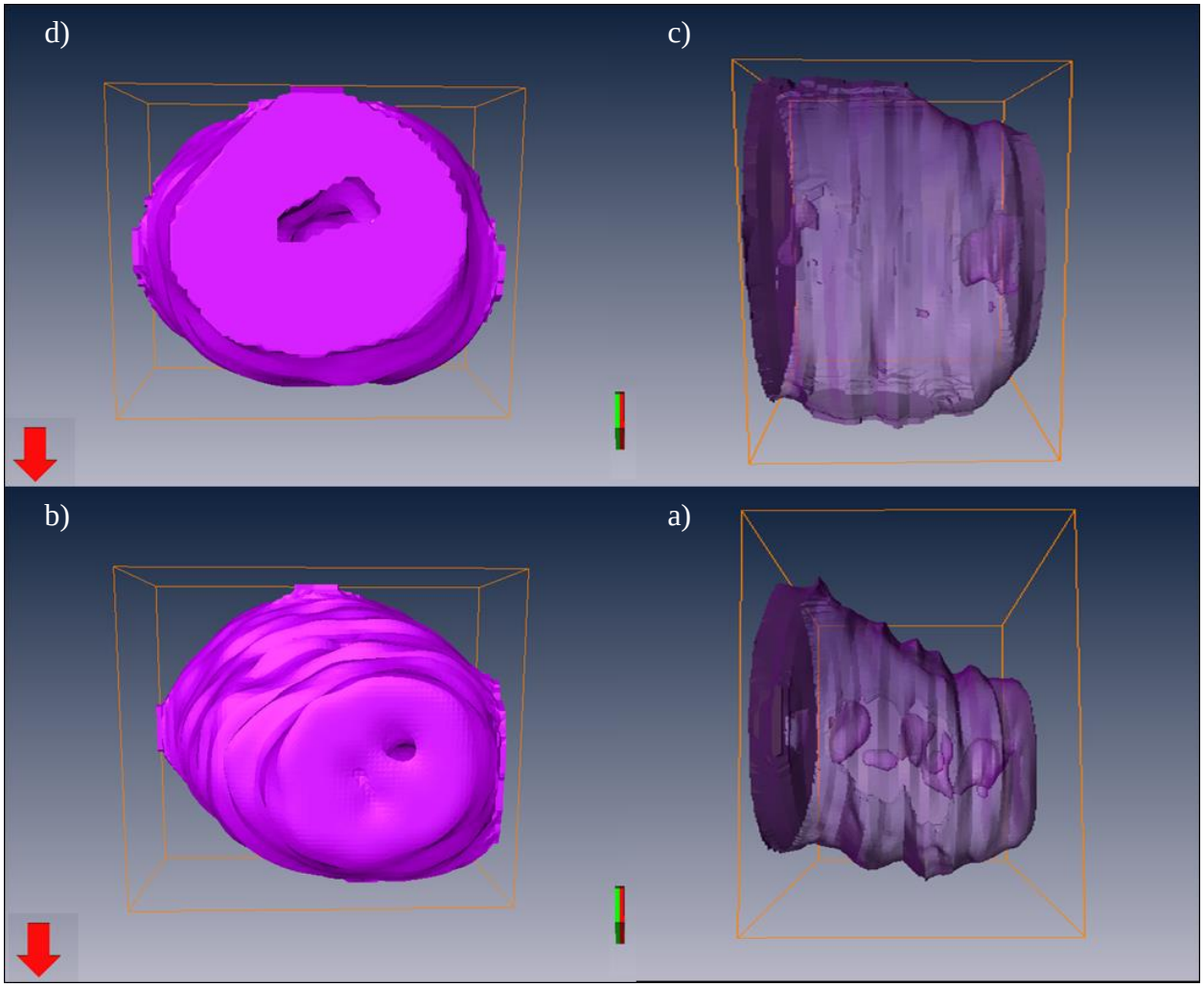

Figure 5. 3D reconstructions for two different Cu nanostructures (upper and bottom rows) corresponding to sample B. Two visual representations of one and the same nanostructure are shown a) and c) in solid color, and b) and c) transparent and rotated by 90 degrees. The surrounding AAO matrix is omitted for clarity.

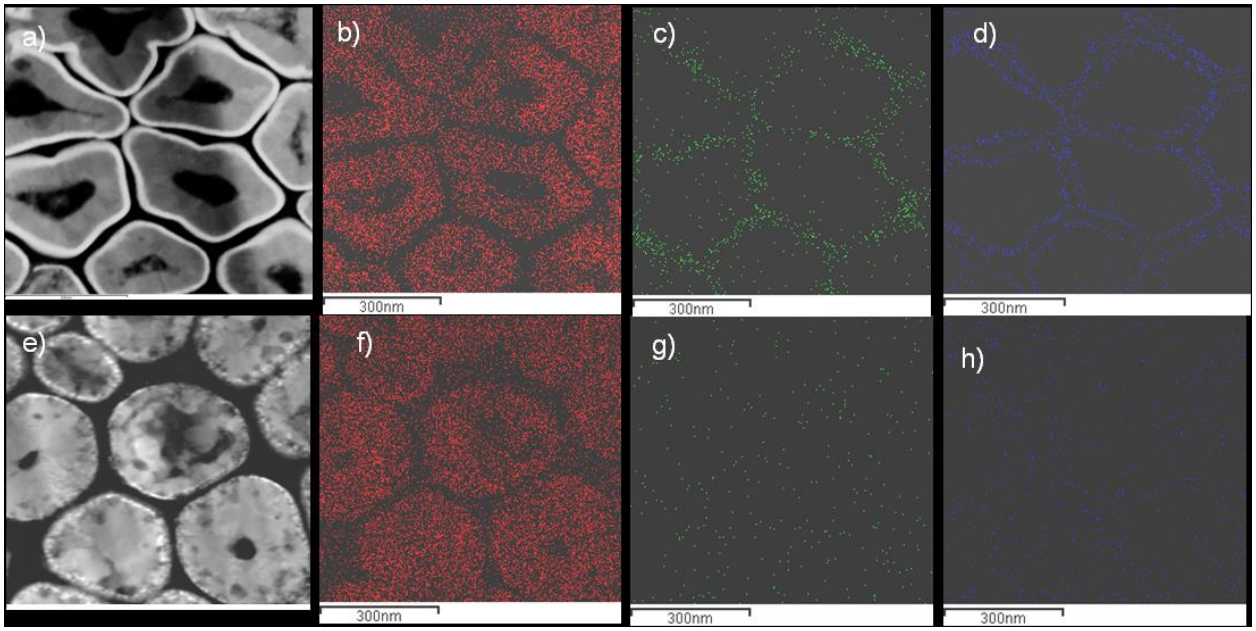

Figure 6. STEM HAADF images for a) sample A and e) sample B whereas the thin foils are extracted from areas at about 150-200 nm away from the back electrode, b) and f) the corresponding EDX Cu mapps, c) and g) the corresponding EDX Al maps and d) and h) the corresponding EDX Au maps.

Supporting Information

S1: Link to movie showing the serial section for sample A The movie is obtained after image registration, alignment and cropping of the original data.

S2: Link to movie showing the serial section for sample B after image registration and alignment. The movie is obtained after image registration, alignment and cropping of the original data.

S3: STEM HAADF image of the sample A whereas the thin foil from an area at about 1000-1100 nm away from the back electrode. Corresponding Cu (blue) and Al (red) EDX maps.